Thin Solid Films 669 (2019) 440–449

Contents lists available at ScienceDirect

Thin Solid Films

journal homepage: www.elsevier.com/locate/tsf

Room temperature ferromagnetism and its correlation to ferroelectricity of manganese embedded in lead zirco-titanate

Ioana Cristina Bucur[a,b], Nicoleta G. Apostol[a], Laura E. Abramiuc[a,b], Liviu C. Tănase[a], Cristian A. Tache[a], George A. Lungu[a], Ruxandra M. Costescu[a], Cristina F. Chirilă[a], Lucian Trupină[a], Lucian Pintilie[a], Cristian M. Teodorescu[a,*]

[a] National Institute of Materials Physics, Atomiștilor 405A, 077125 Măgurele, Ilfov, Romania
[b] Faculty of Physics, University of Bucharest, Atomiștilor 405, 077125 Măgurele, Ilfov, Romania

ARTICLE INFO

Keywords:
Ferroelectrics
Diluted magnetic semiconductors
Indirect exchange
Charge accumulation
X-ray photoelectron spectroscopy
Magneto-optical Kerr effect

ABSTRACT

Manganese is deposited at high temperature on (001) oriented ferroelectric lead zirco-titanate prepared in two different ways: sputter-annealed or just simply annealed in ultrahigh vacuum. Room temperature ferromagnetism (FM) is obtained for Mn deposited on sputter-annealed substrates, while for the other sample preparation a paramagnetic behaviour is obtained. Also, for the first case a clear inwards component of the polarization $P^{(-)}$ is observed by X-ray photoelectron spectroscopy and piezoresponse force microscopy. Composition analysis evidenced formation of Pb vacancies in the case of FM – $P^{(-)}$ sample, consistent with hole formation near the surface, needed both to stabilize the inwards polarization state and to intermediate ferromagnetism between Mn^{2+} ions. The indirect exchange ferromagnetism mediated by holes is stronger, most probably because the interaction energy is proportional with the carrier effective mass. Also, whereas in the case of unsputtered substrate a stable surface Mn oxide is formed, defect formation by sputtering seems to favor Mn migration inside the sample. This also induces the formation of a thin film where ferromagnetism and the orientation of ferroelectric polarization might have the same origin, i. e. holes accumulated near the outer surface.

1. Introduction

A natural wish of the overwhelming part of materials scientists is to link different kind of long range order or correlations between the elementary constituents of matter. In the recent years, the scientific community has witnessed a growing interest in combining ferroelectricity and ferromagnetism due to the potential of engineering new functionalities with applications in microelectronics [1]. 'Multiferroics' exhibiting mutually interdependent ferromagnetism and ferroelectricity constitute an exciting area for both fundamental and applied research. Ferromagnetism and ferroelectricity are partially incompatible, since the first materials require partially filled valence orbitals, while the second require high ionic states of the transition metal (displacive) ion. Moreover, d electrons tend to reduce off-center atomic displacements, which are responsible for permanent dipole moments of unit cells [2]. The only 'natural' multiferroic material, $BiFeO_3$ is in fact a G-type antiferromagnet with quite weak ferromagnetism, if any [3]. Thus, most proposed 'multiferroic heterostructures' couple mechanically two interpenetrating ferroelectric and ferromagnetic phases within different topologies (nanoparticles of phase 1 embedded in phase 2, nanocolumns of phase 1 embedded in phase 2, alternate films of phase 1 and 2) and use the interplay of both ferroelectricity and ferromagnetism with strain (piezoelectricity and magnetostriction, respectively) [3,4].

Several studies of magnetic dopants inside ferroelectric materials were carried out during the last one and a half decade, especially based on $BaTiO_3$ (BTO). A natural scenario to assess the possible occurrence of ferromagnetism is via indirect exchange, using the mean-field Zener [5,6], the oscillating Ruderman-Kittel-Kasuya-Yosida (RKKY) interaction [7–9] or bound magnetic polarons (BMP) [10–12]. One of the main difference between RKKY or Zener models discussed so far and BMP mechanism stems in the nature of charge carriers intermediating the double exchange: in the RKKY or Zener models mainly heavy holes are considered, since the indirect exchange interaction integral is proportional to the effective mass (or, equivalently, to the density states) of the charge carriers [13,14]. In the BMP model, electrons orbiting on large Bohr radius states intermediate coupling between otherwise

* Corresponding author.
E-mail address: teodorescu@infim.ro (C.M. Teodorescu).

https://doi.org/10.1016/j.tsf.2018.11.018
Received 5 June 2018; Received in revised form 4 October 2018; Accepted 9 November 2018
Available online 10 November 2018

insulated magnetic ions found in this spatial region. Nonetheless, all magnetic ion doped BTO results reported so far did not show a clear interplay between ferroelectricity and ferromagnetism [15–19]. Moreover, theoretical studies proposed that, although Cr or Fe are ferromagnetic when diluted into BTO, to render Mn ferromagnetic one needs additional p-type doping [15] while in Ref. 18 the coupling between ferroelectricity and ferromagnetism was reported as weak, and in Ref. 19 the growth conditions (oxygen atmosphere) for obtaining ferroelectric or ferromagnetic Mn-doped BTO are mutually exclusive (elevated O_2 pressure: ferroelectric; reduced O_2 pressure: ferromagnetic). This also could be related to the type of (p, n) doping derived theoretically for synthesis in oxygen (−rich, −poor) conditions [20]. We shall then keep in mind from this short analysis that, irrespective to the doping due to the magnetic impurities themselves, and no matter which is the model used, indirect exchange mediated ferromagnetism is strongly sensitive to the nature of charge carriers in the material.

As for ferroelectricity of thin films which show uniform out-of-plane polarization, it was proven that the stabilization of the single domain ferroelectric state requires compensating charges whose sign clearly depends on the orientation of the polarization [21,22]. These compensation charges may be intrinsic (inside the film) or extrinsic, due to contaminants or ad-layers [23–25], or to metal contacts [26–28]. Pure ferroelectric ultrathin films undergo a sizeable 'self-doping' phenomenon to provide these intrinsic compensation charges [29]. It follows that near the surface of a ferroelectric thin film a considerable charge carrier density is stabilized, whose sign depends on the polarization orientation, according to Fig. 1.

A solution not yet investigated is to use these charge carriers, accumulated near surfaces of ferroelectrics to compensate the depolarization field, to intermediate by indirect exchange the magnetic ordering between separated magnetic ions. This is formally the same mechanism as in diluted magnetic semiconductors, only in this case the processes in question takes place near the surface. From the above analysis of indirect exchange ferromagnetism, we concluded that the presence of ferromagnetic long range order is clearly dependent on the sign of the charge carriers and of their character (bound, free), and these characteristics may occur as a consequence of ferroelectricity. The presence of excess carriers is expected to influence both the magnetic coupling between individual magnetic ions and the polarization orientation, yielding then a new type of surface multiferroicity.

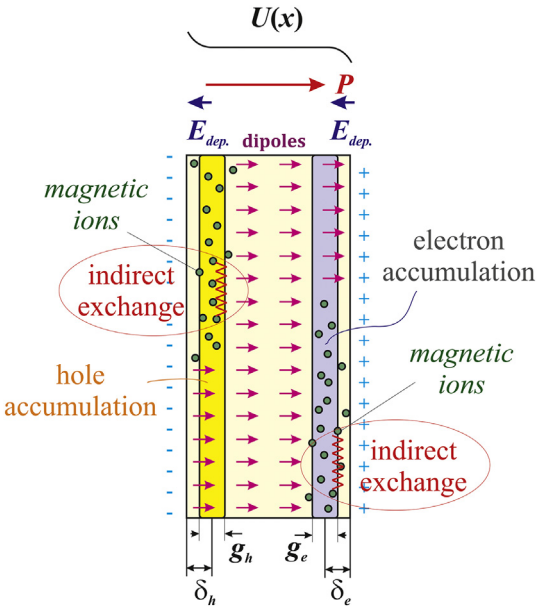

Fig. 1. Electric and magnetic structure of a ferroelectric thin films, for which magnetic ions are placed near each interface. The aligned dipoles produce the polarization P, while their fixed charges at extremities generate the electric depolarization field $E_{dep.}$. Charge carriers from the film are transported by this field near the interfaces such as to form charge sheets able to compensate the depolarization field, such that the electron potential energy inside the film is flat and only at surfaces band bending occurs due to the combined influence of mobile charge sheets and fixed charges. When magnetic ions are diluted with low concentration such as to exclude nearest-neighbor interaction near the surface in a region where mobile charges are accumulated, one expects the onset of magnetic ordering by indirect exchange intermediated by these mobile carriers. It is expected that electron- and hole-mediated ferromagnetism will not yied the same exchange integral. Since the sheet of mobile carriers may be varied by an applied electric field, eventually reversing the polarization, an easy electric control of magnetic properties is expected to manifest.

Clearly, there will be an interplay between the native defects in the ferroelectric (oxygen vacancies) yielding to a sufficient amount of charge carriers to compensate the depolarization field [29] and the charges possibly generated by the embedded magnetic ions themselves. Some previous theoretical [20] and experimental [30] investigations on including Mn into $PbTiO_3$ and $PbZrO_3$ stated that Mn^{2+}/Mn^{3+} substitute Zr^{4+} or Ti^{4+} ions at the B site of ABO_3 perovskite structure as acceptors (although Ref. 20 did not take into consideration spin interactions between Mn atoms) whilst in Ref. 31 the authors claim that below 0.5 mol% concentration of Mn, it is preferentially incorporated in the Pb sites as Mn^{2+}/Mn^{3+}, thus it might have a slight donor character. For larger Mn concentration, Mn^{3+} is incorporated as acceptor on the B site, as determined by electron paramagnetic resonance (EPR). Thus, in most cases, Mn embedded in $PbTiO_3$, $PbZrO_3$ or $Pb(Zr,Ti)O_3(001)$ (PZT) will more likely act as an acceptor, while oxygen vacancies are donors. Thus, conditions are fulfilled to compensate any kind of polarization near surface (electrons are needed to compensate the outwards polarization, holes are needed to compensate inwards polarization [23,24,29], see also Fig. 1) by using Mn together with variable stoichiometry perovskites $ABO_{3-\delta}$. Moreover, a clear interplay was recently reported between the polarization state (and the associated self-doping) and the interfacial (conduction, work function) properties of the substrate [32,33]; the surface ferroic properties are expected to be influenced also by the bottom interface, and then an additional way of controlling these properties is expected.

The aim of this paper is to discuss the first experimental evidence of such a phenomenon. Manganese was deposited on thin films of lead zirco-titanate (PZT) thin films which were proven to exhibit out-of-plane polarization by piezoresponsive force microscopy (PFM) and X-ray photoelectron spectroscopy (XPS; see below). To enhance manganese diffusion inside the perovskite, the deposition took place at high temperature (400 °C), as in the case of Fe [34] or Mn [35,36] deposited in Ge(001) whose lattice constant is quite close to that of PZT. The PZT(001) thin film was prepared just by annealing in ultrahigh vacuum (UHV), this procedure being known to produce oxygen vacancies [29,37] or was Ar^+ pre-sputtered before annealing, in order to increase the number of defects, possibly cations, near surface. Oxygen vacancies behave as donors, freeing electrons which may be used by the ferroelectric thin film to compensate the fixed charges and set its single domain polarization state [29], while cation vacancies will act as acceptors [24]. X-ray photoelectron spectroscopy is used to quantify: (i) the composition of the substrate; (ii) its polarization, via the band bending exhibited by core levels near surface [27,29,37–45]; (iii) the quantity and chemical state of manganese deposited, together with possible changes in the polarization of the substrate. PFM is used to confirm the XPS data and to help in the interpretation of the different XPS components. Moreover, XPS is extremely surface sensitive and is commonly used to quantify ad-layers at the monolayer level [45]. Ferromagnetism at room temperature is analyzed by magneto-optical Kerr effect (MOKE). It will be shown that the occurrence of room temperature ferromagnetism is strongly dependent on the initial polarization state and hence on the preparation procedure.

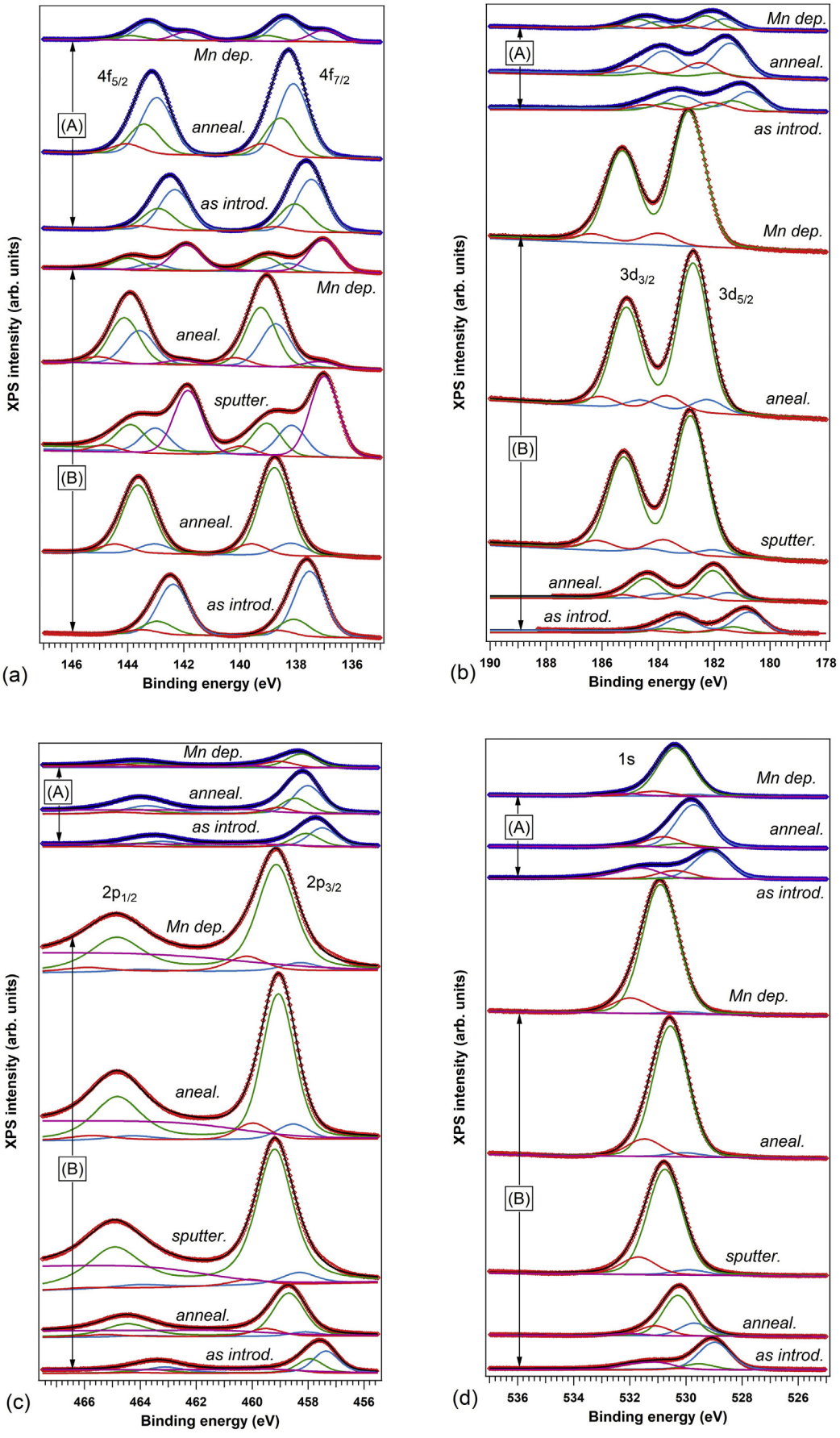

Fig. 2. X-ray photoelectron spectra from the substrate core levels: (a) Pb 4 f; (b) Zr 3d; (c) Ti 2p; (d) O 1 s. (A), red symbols: a PZT(001) film as introduced, after annealing to remove contaminants, and after the equivalent of 20 nm Mn deposited at 400 °C; (B) another PZT(001) film as introduced, annealed, then sputtered with Ar^+ ions (1 μA, 20 min), then again annealed and with the same quantity of Mn deposited. The spectra are simulated with doublets constituted by Voigt lines separated by the spin-orbit splitting and with intensity ratios defined by the branching ratio, together with associated inelastic backgrounds. The relative separation between components is kept constant amongst all four core levels, with the exception of the additional, low binding energy component for Pb 4 f. (For interpretation of the references to colour in this figure legend, the reader is referred to the web version of this article.)

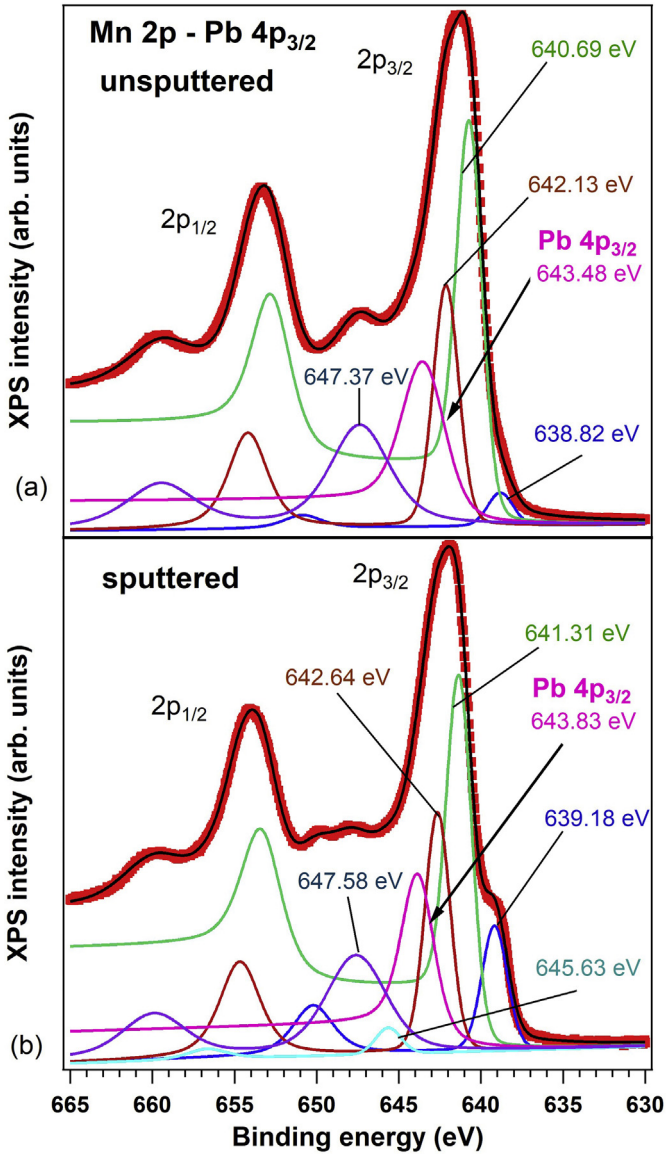

Fig. 3. Mn 2p X-ray photoelectron spectra for Mn/PZT(001) deposited at high temperature on (a) unsputtered and (b) sputtered substrates. Spectra are deconvoluted by using spin-orbit split doublets with associated inelastic background, plus one singlet to account for Pb $4p_{3/2}$ core level, which is found in this energy range. The $2p_{3/2}$ binding energies for each component are specified by using similar colors as the corresponding curves.

2. Experimental aspects

150 nm thick PZT(001) films are grown on 20 nm $SrRuO_3$ deposited on $SrTiO_3$(001) by pulsed laser deposition (PLD, manufactured by Surface) according to the procedure described in more details in Refs. [24, 27, 29, 40]. This thickness was chosen such as to be in the range of the attenuation length of the red laser light used for MOKE measurements (absorption coefficient of about $6 \times 10^6\,m^{-1}$ [46]), assuming that the whole PZT would eventually become magnetic, in order to maximize any possible magnetic signal detected in this first experiment. Performing similar experiments with various PZT thicknesses is the subject of further investigations planned for the future. The PZT films showed good crystallinity and epitaxial quality, as checked by X-ray diffraction and high resolution transmission electron microscopy (HRTEM), and their polarization state was investigated by piezoresponse force microscopy and by ferroelectric hysteresis cycles. Refs. [26, 29, 32, 44] present more details of such investigations. These films are then transferred into a surface science cluster (manufactured by Specs), which comprises a molecular beam epitaxy (MBE) for sample preparation and a chamber for analysis by photoelectron spectroscopy. Contaminants on these films are typically removed by annealing in UHV at a base pressure into the 10^{-10} hPa range, and at a temperature of 400 °C, during three hours. This results in oxygen vacancies and the setup of a single domain polarization state, oriented outwards. Oxygen vacancies produce electrons to screen the depolarization field at the outer surface, according to Fig. 1 [18]. Moreover, recently such films with thicknesses up to 100 nm showed clear 1 × 1 low energy electron diffraction (LEED) patterns, when annealed in oxygen, together with the setting of a single domain polarization state oriented inwards [45]. In this case, the positive charge sheet needed for compensation may equally be formed by holes produced by cation vacancies or by positively ionized donors (oxygen vacancies). However, for the films analyzed in the follwing we preferred to choose another method to control the polarization state, by pre-sputtering the films before Mn deposition. As will be demonstrated below, this has also the advantage to enhance Mn diffusion inside the ferroelectric PZT. Thus, one series of experiments was conducted on just annealed PZT(001), while a second series of experiments dealed with a PZT(001) annealed, then Ar^+ sputtered 6 min in a base pressure of 10^{-7} hPa, 1 kV acceleration voltage, ~4 μA ion current, using a differentially-pumped Specs IQE 12/38 ion gun. Manganese was deposited in a base pressure of 1×10^{-9} hPa, by using a custom made Knudsen cell with direct heating through the walls of the oven, made of thin Ta tubes. The quantity of Mn deposited is the equivalent of a 20 nm thick pure Mn film, as calibrated by a quartz thickness monitor. This quantity of Mn was chosen such as to promote in average about 7.5% atomic density of manganese when related to the thickness of the PZT film (note that the atomic densities in bulk Mn and PZT are similar up to a difference of a few percents). This atomic density range within the limits for ferromagnetism occurence in Mn-based diluted magnetic semiconductors.

XPS measurements were performed in ultra high vacuum (UHV), using a monochromatized Al K_α source (1486.74 eV). For achieving sample neutralization during XPS measurement, a flood gun operating at 1 eV acceleration energy and 0.1 mA electron current were used. More details about the system were discussed in Ref. [37]. XPS data are analyzed by ‚deconvolution' using Voigt profiles [47–49], separate inelastic backgrounds associated to each component in order to discriminate between the bulk and surface components [50]. The latter Ref. also gives the formulas used for fitting. For the Ti 2p spectra, different Lorentz linewidths are used for $2p_{3/2}$ and $2p_{1/2}$ to account for Coster-Kronig processes [51], together with a broad singlet to account for a superposing Pb Auger line [26,40].

The magnetic properties of these samples were investigated at room temperature by longitudinal magneto-optical Kerr effect (MOKE) in an AMACC Anderberg and Modeer Accelerator AB system with a diode laser (λ = 632 nm), at a maximum applied field of 0.25 T. Surface morphology and ferroelectric properties are also investigated by atomic force microscopy (AFM) and piezoresponse force microscopy (PFM) by using a MFP-3D Asylum Research setup. The polarization of the film is determined by pre-poling some area of the surface with inwards and outwards polarization according to a pre-defined pattern and by comparing the phase of the oscillating voltage applied to the tip on areas of unknown polarization with that obtained from the poled areas.

3. Results

XPS spectra of Pb 4 f, Zr 3d, Ti 2p and O 1 s are presented in Fig. 2(a–d), in this order. For all these figures, region (A) with data presented as blue symbols presents spectra obtained for a unsputtered film: the as-introduced film, the film after annealing for 3 h at 400 °C and for the film after Mn deposition with the substrate held at 400 °C. The region (B), red symbols, for all four figures, contains five spectra: as-introduced, after a first annealing (3 h, 400 °C) in UHV, after

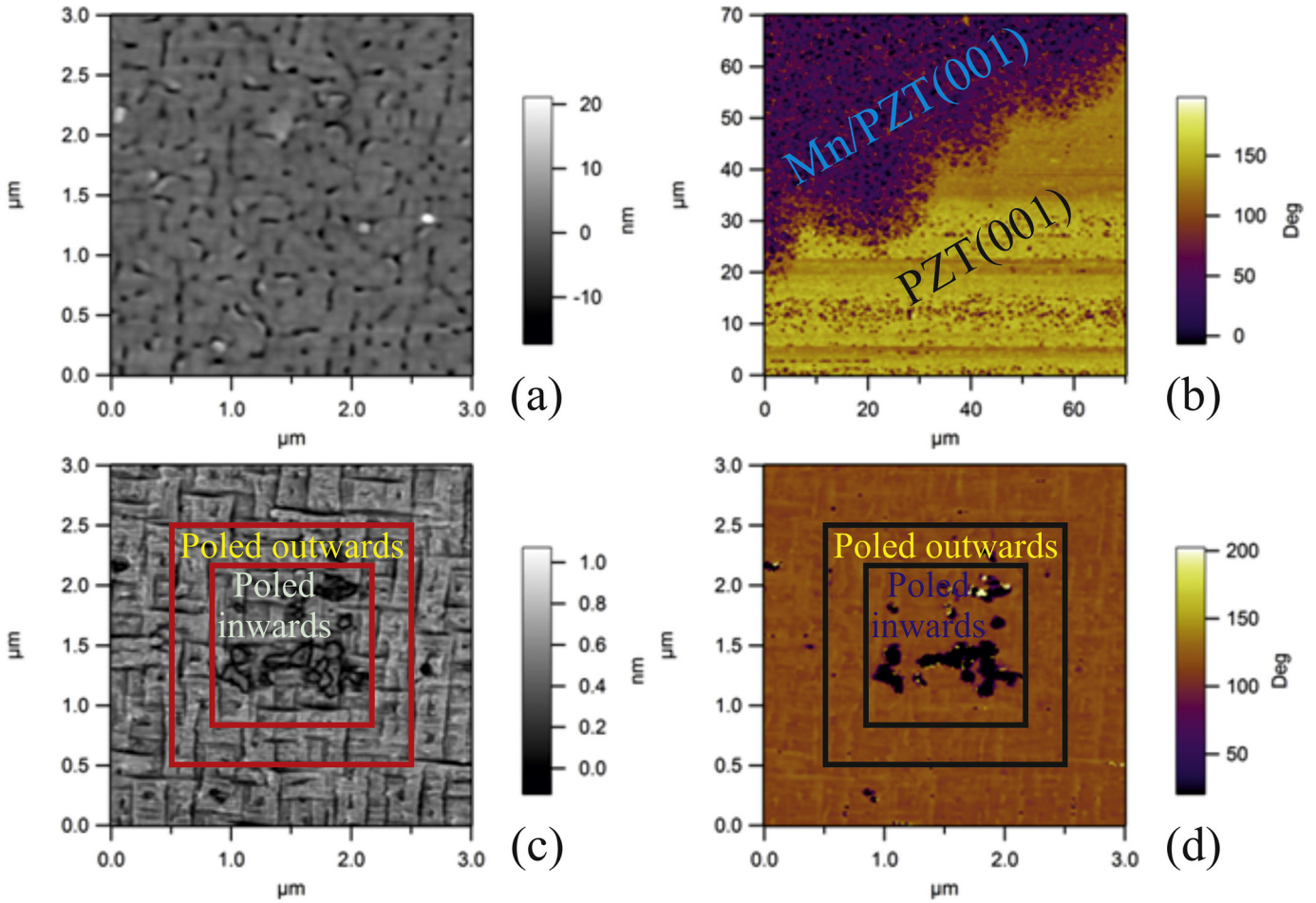

Fig. 4. Scanning probe microscopy results for the sample (b), i. e. the one which was subject to sputtering prior to Mn deposition: (a) topography (atomic force microscopy) on a PZT(001) area without Mn deposited; (b) Phase signal from piezoresponse force microscopy (PFM) between areas with and without Mn deposition (the latter one was shadowed by the sample fixation clamps); (c) PFM amplitude and (d) PFM phase signal from a PZT(001) area without Mn deposited, after poling the film following the map represented in both figures. The region of the sample from (c, d) is the same as for (a).

sputtering (1 kV, ~4 μA, 6 min), again after annealing and after Mn deposition on heated substrate at 400 °C. Mn 2p spectra are represented in Fig. 3 and one may notice that the Pb $4p_{3/2}$ line is mixed with the Mn 2p doublet, thus the analysis by ‚deconvolution' was mandatory to separate this contribution. The main Mn 2p components which will be used for composition analysis are as follows: the most intense component yields at $2p_{3/2}$ binding energies of ~ 640.7 eV for the unsputtered sample and at ~ 641.3 eV for the sputtered sample, represented by the green curve in Fig. 4. This corresponds most likely to Mn^{2+} [52–54], and the fact that it is shifted towards higher binding energies in the sputtered sample might be related either to a different chemical environment, or to some polarization effects. It may also happen that this main line in the sputtered sample corresponds to Mn^{3+} (641.9 eV [52,54]), red shifted by polarization effects. The component at a higher binding energy ~ 642.1 eV in the unsputtered sample and ~ 642.6 eV in the sputtered sample corresponds to Mn^{4+} (642.2 eV according to Ref. [52] and 642.6 eV according to Ref. [54]) and this is maybe slightly red shifted in the unsputtered sample by polarization effects. The peak at lowest binding energy, whose relative intensity is considerably increased in the sputtered sample, agrees well with metal Mn (639.2 eV according to Ref. [53]), but it might also be ascribed to Mn^{2+} present on areas with strong inwards polarization. Owing to the high oxidation potential of manganese, formation of metal Mn when deposited on an oxide is rather unlikely. Note that the typical uncertainty in binding energy derivation by deconvolution is about 0.01 eV.

According to the surface band bending considerations for ferroelectric thin films [24,26,29,33,38–45], areas with different polarizations are expected to manifest in XPS as rigid surface band bendings. For clean samples (i. e. no outer layers which may stabilize compensating charges), in order of increasing binding energy, the respective components are: inwards polarization $P^{(-)}$, no out-of-plane polarization $P^{(0)}$, and outwards polarization $P^{(+)}$, with a separation of 0.6–1.1 eV between adjacent polarization states [24,33,40–42,45]. Thus, one novelty for the fitting procedure presented in this paper is that *all four core levels are fit simultaneously*, by using the same relative binding energies between components ascribed to different polarization states and observing the amplitude ratio to not show too many differences from one core level to another. Some differences between amplitude ratios are, however, acceptable owing to different photoelectron inelastic mean free paths (IMFP) and to photoelectron diffraction effects [55]. Nonetheless, for some Pb 4 f spectra this procedure did not result in good fits; thus, one additional, low binding energy (LBE) component was needed for the sputtered sample after sputtering, annealing and Mn deposition and also for the unsputtered sample after Mn deposition. We may from the beginning anticipate that this component might be related to $P^{(-)}$ polarization; more comments on it will be provided in the next Section. Also, the O 1 s spectra for *as introduced* samples were supplemented with two high binding energy components 530.9 and 532.7 eV to account for C═O and O−C═O contaminants [56]. These components were not considered in the atomic composition ratios listed in Table 1.

Surface compositions are derived after 'deconvolution' by using

Table 1
Composition analysis from the analysis of XPS spectra represented in Figs. 2 and 3. Total integral intensities are used, with the exception of the O 1 s components with binding energy larger than 531 eV, which are due to contaminants. Also, for Mn 2p analysis, only the first three components in order of increasing binding energy are used, i. e. the Pb $4p_{3/2}$ line and the Mn 2p satellites are excluded. The integral intensities are normalized by the Wagner empirical atomic sensitivity factors [57]. Composition error bar: typically ± 2%.

Sample	State	Pb 4 f (LBE)/total	Pb/(Zr + Ti)	O/(Zr + Ti)	Zr/(Zr + Ti)	Mn/(Zr + Ti)
(A)	As introduced	–	1.08	3.44	0.29	–
	Annealed	–	1.11	3.67	0.42	–
	Mn deposited	0.285	0.81	8.77	0.29	5.73
(B)	As introduced		1.19	3.20	0.23	–
	Annealed		0.93	3.29	0.21	–
	Sputtered	0.532	0.33	2.21	0.22	–
	Annealed	0.054	0.28	2.66	0.24	–
	Mn deposited	0.568	0.15	2.93	0.24	0.85

integrated amplitudes together with atomic sensitivity factors [57]. Some results for atomic ratios are represented in Table 1, by taking into account all three components for all substrate core level spectra, plus the LBE for Pb 4 f. For Mn 2p, only the first three components in order of increasing binding energy were used for atomic composition ratios, without the Pb $4p_{3/2}$ line and the high binding energy shake-up satellites. It seems that annealed samples are almost stoichiometric, with a slight oxygen enrichment, but this can also be due to some mixing with components corresponding to some contamination in the range of 529–530 eV binding energy (e. g. adsorbed hydroxyls [54,56]). The surface contamination level, estimated by quantifying the C:O(PZT) ratio between the C 1 s XPS intensity (not shown) and the intensity of the main component in O 1 s spectra (see Fig. 2(d)), is of about one C atom for 30 $Å^2$ for the unsputtered sample after annealing and Mn deposition, and about one C atom for 40 $Å^2$ for the sputtered sample after sputtering, annealing and Mn deposition. This is estimated by starting with the oxygen ‚effective' density of about 9 atoms for a surface unit cell of about 15 $Å^2$. (The 9 oxygen atoms are about 3 for each unit cell, and one takes into account that the equivalent investigated depth for O 1 s electrons with about 960 eV kinetic energy is about 3 unit cells, the equivalent of ~ 12 Å, the IMFP for these electrons [40].) Thus, in the following we shall rule out the doping effect of these contaminants, since their quantity is far lower than that of oxygen or cation vacancies, or of Mn atoms.

After Mn deposition on the unsputtered sample, the sample composition changes drastically in the sense that the ratio between the oxygen signal and any cationic signal from the substrate increases drastically. The only way to interpret this phenomenon is the formation of a surface Mn oxide. Indeed, ruling out IMFP effects, the surface composition may be written approximately as $Pb_{0.8}Zr_{0.3}Ti_{0.7}O3$ + 5.7 MnO. In fact, one may assume that MnO is formed on the PZT surface and estimate its thickness θ(MnO), by assuming in a simplified model that all IMFP are similar (λ ≈ 1.6 nm) such as $\theta(\mathrm{MnO}) \approx \lambda \ln\{1 + I(\mathrm{MnO})/I(\mathrm{PZT})\} \approx 3$ nm. The remaining part of Mn probably diffuses deeper inside the PZT film. These Mn donors, probably together with Pb vacancies (~ 0.2 per formula unit in the outer layer) create holes necessary to stabilize on some areas the $P^{(-)}$ polarization state, visible from the LBE component of Pb 4 f.

For the sputtered sample, immediately after sputtering, the Pb content decreases drastically near surface. This happens together with the installation of a strong LBE component, thus Pb vacancies produce holes which stabilize on some areas the inwards polarization state $P^{(-)}$. After annealing, the relative weight of the LBE component decreases, nevertheless, it is still preset together with a low content of Pb per formula unit near surface. Mn deposition reinforces again the Pb LBE component, to a much stronger extent than in the case of the unsputtered sample.

Another hint about the Mn diffusion may be traced by looking to two different Mn core levels, Mn 2p and Mn 3p, producing photoelectrons with different kinetic energies (about 845 eV and 1438 eV, respectively, from the survey scans) and hence with different IMFPs. These may be approximated, in monolayers, as $0.41\sqrt{aE(\mathrm{eV})}$, where a is the interplanar spacing corresponding to one monolayer and E is the electron kinetic energy [58]. With $a \approx 2$ Å, IMFPs of 10.7 and 13.9 Å are obtained for Mn 2p and Mn 3p excited with Al K_α. If the Mn concentration is constant, the ratio between the integral intensities, corrected by the atomic sensitivity factors, should yield $I(3p)/I(2p) \approx 1.3$. From the actual photoemission data, from the survey scans, we insulated the Mn 2p and Mn 3p levels, extracted double Shirley backgrounds, then computed their integrals and the net result was $I(3p)/I(2p) \approx 1.23$ for the sputtered sample and ≈ 1.09 for the unsputtered sample. The next step was to simulate a linear Mn concentration decrease from the surface towards the bulk of PZT, such as $n(z) = n_0(1 - c \cdot z)$, z being the coordinate along the $[00\bar{1}]$ direction. The intensity ratio between two core levels with different IMFPs λ_1 and λ_2 may be expressed as:

$$\frac{I_1}{I_2} = \frac{\int_0^\infty n(z)\exp\left(-\frac{z}{\lambda_1}\right)dz}{\int_0^\infty n(z)\exp\left(-\frac{z}{\lambda_2}\right)dz} = \frac{\lambda_1}{\lambda_2}\bullet\frac{1 - c\bullet\lambda_1}{1 - c\bullet\lambda_2} \quad (1)$$

Knowing the IMFPs and the intensity ratios, the above equation may be reversed to yield the decay coefficient $c \approx 1.5 \times 10^{-2}$ $Å^{-1}$ for the sputtered sample and 3.3×10^{-2} $Å^{-1}$ for the unsputtered sample. These estimates, of course, are valid only within a few IMFPs near surface (3–4 nm) and within this oversimplified model. However, immediately near surface the decrease in Mn concentration is rather slow, especially for the sputtered samples, where the decay is about 15% for 1 nm depth. The question of Mn distribution inside the PZT film is highly important and this will be tackled by analytical high resolution transmission electron microscopy in the near future.

Fig. 4 presents PFM data obtained for the sputtered sample, after Mn deposition and extraction to ambient atmosphere. PFM data for the fresh unsputtered sample are already published in Ref. [28], since the sample used for this study and for the actual one resulted from cutting the same PZT/SRO/STO(001) crystal. This investigation yielded the coexistence of both $P^{(-)}$ and $P^{(+)}$ orientation was prior to Pt deposition (in Ref. [28]) or Mn deposition (in the actual study). After poling with ± 10 V (i. e. ± 6.7×10^8 Vm^{-1} applied field) according to a predefined pattern, both poled areas remained stable. Back to the sputtered sample, one observes the prevalence of the $P^{(+)}$ polarization on areas without sputtering and Mn deposition (areas masked by the fixation clamps). The PLD preparation conditions for this sample were the same as from the sample discussed in Ref. [28]; thus, one may affirm that both samples are similar, with the exception of a slightly different Zr content, according to Table 1. Thus, annealing the actual sample yielded a stable $P^{(+)}$ state over the whole surface, while areas with $P^{(-)}$ poling are unstable within a few minutes, as can be seen from Fig. 4(c, d). But the most important finding is obtained on areas representing transition from the just annealed surface and the surface which was subject to sputtering and Mn deposition. It is clear that the polarization state on these two areas represented in Fig. 4(b) is different and by

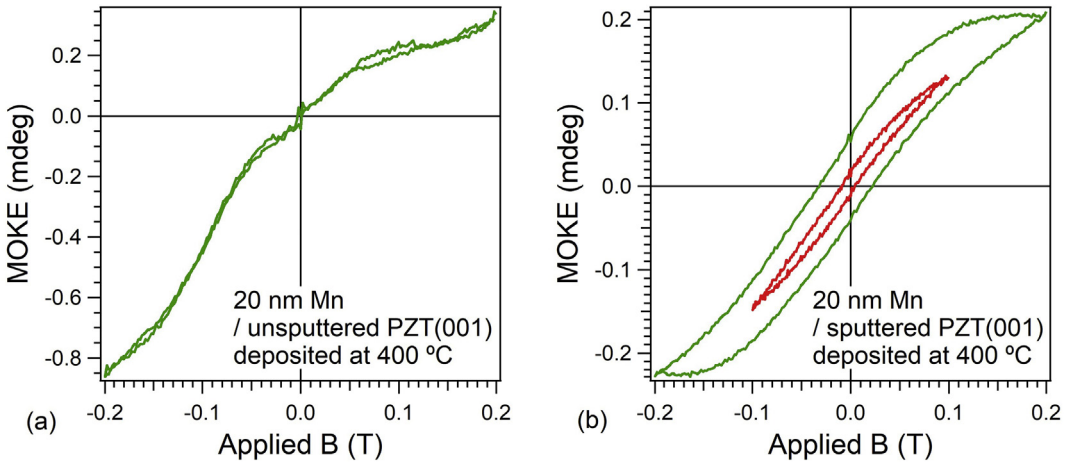

Fig. 5. Magneto-optical Kerr effect measurements on (a) the equivalent of 20 nm Mn deposited at high temperature on a PZT(001) film, previously sputtered and annealed; (b) the same amount of Mn deposited at the same temperature on a PZT(001) film subject just to annealing in ultrahigh vacuum. The corresponding XPS spectra are represented in Figs. 2–6. In (b), also a minor hysteresis cycle was represented.

comparing with the other phase signals one may infer that the area which was subject to sputtering + Mn deposition presents inwards ($P^{(-)}$) polarization.

Fig. 5 presents MOKE data obtained at room temperature. It is straightforward that the unsputtered sample behaves as a paramagnet, whereas a ferromagnetic hysteresis cycle is recorded for the sample with sputtering and annealing prior to Mn deposition. For estimating the magnitude of the Mn magnetic moment, one uses a calibration such as 2.5 ± 0.5 mdeg corresponds to 1 nm of bulk Fe with 2.2 Bohr magnetons per atom, or a magnetization of 1.7×10^7 Am^{-1} [59–61]. In the actual case, the saturation magnetization is about ten times lower. The Mn atomic density, as derived by XPS (Table 1) is about $0.85/64$ $Å^3 \approx 1.3 \times 10^{28}$ m^{-3}, while the atomic density of bulk Fe is about $2/(2.87$ $Å)^3 \approx 8.5 \times 10^{28}$ m^{-3}. Thus, the average Mn atomic moment is $2.2 \times (8.5/1.3)/10 \approx 1.4$ Bohr magnetons. This is in the upper range of values listed by Coey in Ref. 10, also this corresponds to $0.85/5 = 17$ at. % and *is obtained at room temperature*. This value is higher than the Fe magnetic moment embedded in Ge(001) [34] and the saturation magnetization is about one half from the Mn ferromagnetic signal also embedded in Ge(001) [35,36], however with Mn concentration of about 0.27–0.36 at. % [35]; at the end, the Mn atomic magnetic moment is similar in the actual study and in Refs. 35, 36. Also, these values are higher than the lowest temperature (4.2 K) ones recorded for Mn diffused into InAs(001), which was about 0.7 Bohr magnetons [62]. Hence, the result from Fig. 5(b) is remarkable from the point of view of magnetism only, not to speak also about its possible interplay with ferroelectric properties. We shall see in the next Section that even higher values of the Mn magnetic moment may be supposed, if the thickness of the ferromagnetic layer is supposed lower.

One needs, however, to be careful with such data obtained on novel systems, since it was proven that nanostructuring, interface (e. g. core-shell) effects or oxygen vacancies (i. e. partial reduction of components from the initially nonmagnetic insulating sample) may induce ferromagnetic ordering [63,64]. However, the order of magnitude of the magnetization of these samples is in the range of 200–300 Am^{-1}, about three orders of magnitude lower than the actual values derived from the present MOKE data. Bare PZT samples were checked by MOKE and did not yield a measurable ferromagnetic signal at room temperature. The sputter-annealed PZT samples were not checked by MOKE, but the lack of reduced components (e. g. Ti^{3+}, Zr^{3+}) in XPS pushes us to consider that the strong observed ferromagnetic signal is due to manganese, in line with the assumptions of Ref. 19.

In the following Section we will detail more about the possible origins of the observed ferromagnetism and on its interplay with sample preparation procedure and ferroelectricity.

4. Discussion

It seems fairly clear that the occurrence of ferromagnetism might be related to the stabilization of inwards polarized state $P^{(-)}$, as revealed by PFM. A fingerprint of the inwards polarization is the LBE XPS component for Pb 4 f, whose 4 $f_{7/2}$ binding energy (137.05 ± 0.10 eV) is quite similar to the certified $P^{(-)}$ polarization reported in Refs. 24 (137.25 eV) and 45 (137.29 ± 0.04 eV amongst all three sample thicknesses analyzed). However, the rigid band bending should manifest also in the other core level positions, especially in cases where the δ_h parameter (distance from the surface to the center of the distribution of the accumulated holes, see Fig. 1) is in the range of a few nanometers [22], higher or at least comparable with the IMFP. In Ref. 45 it was also found that this parameter should be considerably lower than the value derived more than one decade ago from electrical measurements [22]; it might be in the range of half of the unit cell, about 2 Å, at least for for $P^{(-)}$ states. In this case, assuming that samples are PbO terminated, only the outer layer should experience the band bending due to polarization. But, in this case also the O 1 s should exhibit a low binding energy component, whereas such a component was not visible in XPS spectra. Note that in both Refs. 24 and 45 the O 1 s component for $P^{(-)}$ states yields at 528.74 ± 0.06 eV, while from the actual data the lowest binding energy component of O 1 s yields at 529.91 ± 0.17 eV, i. e. larger by > 1 eV. The fact that no O 1 s LBE component is visible by XPS in these samples (A after Mn deposition; B after sputtering, annealing and Mn deposition) pushes us to find an explanation, while still assuming that the LBE Pb 4 f signal belongs to the $P^{(-)}$ polarization state. There should be a mechanism which compensate the expected red shifting of O 1 s due to the surface polarization. The most likely mechanism should be related to the fact that all these samples exhibited Pb deficit in the outer layers, according to Table 1. Thus, in average the O atoms will be less negatively charged and therefore are expected to shift at higher binding energies; this shift could compensate the shift due to the surface band bending. To quantify these effects, we took into consideration the relative O 1 s shift from similar compounds with different cationic states. Performing a statistical analysis of all O 1 s data from the NIST database [54] for titanium oxides, O 1 s in TiO_2 yields at 529.95 ± 0.25 eV, and in Ti_2O_3 at 530.45 ± 0.85 eV if one takes into account both listed data by NIST, or 531.3 eV if one takes into account only the most recent paper on this subject [65]. Consequently, about 1 eV shift towards higher binding energies is likely to occur owing to cation vacancies in these surface layers. This might be an explanation for the absence of the LBE component of O 1 s related to the surface band bending. Note also that in Refs. 24 and 45, the sample surfaces were nearly stoichiometric, thus this blue shifting effect on O 1 s signal

is not expected to occur.

To preclude other than polarization-related origin of the Pb 4 f LBE component one has to compare it with metal Pb disrupted from the PZT surface occurring at ~ 136 eV in Ref. 38 or ~ 136.5 eV in Ref. 43 (the 4 $f_{7/2}$ line). In Refs. 43 and 44 it was found that metal Pb may be ejected from the PZT film only by intense soft X-ray irradiation with extremely focused synchrotron radiation. On the other hand, vigorous substrate disruption was reported following transition metal deposition in Fe/GaAs [66–68] and in Fe/InAs [47,48,68]. Also, metal Pb is ejected from the PZT thin film when Cu or Au are deposited by RF magnetron sputtering, while Ag deposition by using an effusion cell yielded a lower substrate disruption [38]. If we assume that the Pb 4 f LBE component is due to the ejection of metal Pb induced by Mn deposition, still one needs to explain why its binding energy is higher by at least 1 eV. One may assume, for example, that this metal Pb is formed on areas with outwards ($P^{(+)}$) polarization. Thus, these Mn-containing samples and also the sputtered surfaces may be described as being PZT with outwards polarization with some metal Pb on top. On one hand, the Pb—O bond is about 1.8–1.9 times stronger than the As—Ga or As—In bonds [69]. On the other hand, no such surface disruption was reported when Cu [26,32,42], Au [26,32,40,41] or Pt [28] are deposited on PZT in our setup, by using effusion cells. Finally, the PFM data clearly shows that the surfaces obtained after sputtering, annealing and Mn deposition exhibit inwards polarization. Thus, this second scenario of substrate disruption and formation of metal Pb onto outwards polarized surfaces will be discarded in favor of the first scenario, consisting in (i) formation of areas with inwards polarization, (ii) abrupt band bending such that it manifests only for the outer atomic layer, which in turn shows (iii) Pb deficit and hence the O 1 s core level from this outer layer experiences, in addition to the LBE shift due to band bending, also a blue shift due to less cationic coordination.

Before connecting definitively, the occurrence of ferromagnetism to the inwards polarized state of the film, one needs to take into consideration also possible (hetero)structural effects. In the previous Section, from the composition analysis it was inferred that the unsputtered sample might be regarded as being formed by a relatively thick (~ 3 nm) MnO film deposited on PZT. This outer film is not ferromagnetic, and also from the bulk one cannot detect any ferromagnetism, knowing that the probing depth of the MOKE method is about 15–20 nm [59,60].

Hence, the observed ferromagnetism is likely to be connected to the $P^{(-)}$ polarization, and thus the charge carriers responsible for this ferromagnetism are holes. The ferromagnetic sample exhibit a noticeable Pb deficit (Table 1) and an important Mn concentration, in total its concentration near surface being ~ $Mn_{0.85}Pb_{0.15}Zr_{0.24}Ti_{0.76}O_{2.93}$. The donor or acceptor character of Mn^{2+} on Pb sites is difficult to be ascribed, but nevertheless Mn^{2+} on (Zr,Ti) sites is clearly an acceptor; on the other hand, Pb vacancies are acceptors with impurity levels close to the maximum of the valence band [70]. Thus, one may consider, as a first approximation, that in absence of the surface band bending, the Fermi level is pinned to the $Pb_{vac.}$ impurity level, close to the maximum of the valence band. Therefore, a band bending near surface such that represented in Fig. 1 will induce a hole accumulation with a maximum density, in the free particle approximation:

$$p_{max.} = \frac{1}{3\pi^2}\left(\frac{2m^*\Delta\varepsilon}{\hbar^2}\right)^{3/2} \quad (2)$$

where $\Delta\varepsilon$ is on the order of the total band bending. An average density which may be computed by using the density of states $g \sim \varepsilon^{1/2}$, yielding $p_{avg.} = p_{max.}/2$. With a band bending $\Delta\varepsilon \approx 1$ eV and a hole effective mass m^* equal to the free electron mass, $p_{max.} \approx 4.5 \times 10^{27}\,m^{-3}$, $p_{avg.} \approx 2.3 \times 10^{27}\,m^{-3}$. This is a high carrier density, the semiconductor is degenerated and one may then use the RKKY formalism. The RKKY exchange integral between two spins S_1 and S_2 may be written as [7,14]:

$$J_{12}(R_{12}) = -\frac{|\Delta|^2 m^*}{8\pi\hbar^2 {R_{12}}^4}\{2k_F R_{12}\cos(2k_F R_{12}) - \sin(2k_F R_{12})\} \quad (3)$$

where k_F is the Fermi wavevector, $k_F = (3\pi^2 p)^{1/3}$ in the free particle approximation, R_{12} is the distance between the two spins, approximated as $\{3/(4\pi n_i)\}^{1/3}$, where n_i is the density of magnetic impurities, and $|\Delta|$ is the matrix element of the exchange interaction by using impurity core ϕ_0 and delocalized Bloch function at the maximum kinetic energy ϕ_{kF}:

$$\Delta = \int d^3r d^3r' \frac{e^2 {\phi_0}^*(r'){\phi_{k_F}}^*(r)\phi_0(r)\phi_{k_F}(r')}{4\pi\epsilon_0\,|r - r'|} \quad (4)$$

Note that the wavefunctions are not normalized to unity, but to the square root of the crystal volume, in the original treatment of Ref. [7]. Thus, the parameter Δ is measured in units of energy × volume. The interaction energy between both spins is $-J_{12}S_1S_2$, thus positive J's correspond to parallel ordering of spins S_1, S_2. This exchange integral may be written in terms of the hole and impurity densities:

$$J_{12} = -\left(\frac{\pi}{162}\right)^{1/3}\frac{|\Delta|^2 m^* {n_i}^{4/3}}{h^2}\left\{\left(\frac{18\pi p}{n_i}\right)^{1/3} cos\left[\left(\frac{18\pi p}{n_i}\right)^{1/3}\right] - sin\left[\left(\frac{18\pi p}{n_i}\right)^{1/3}\right]\right\} \quad (5)$$

Ferromagnetism, i. e. positive values of J_{12} are achieved for $p/n_i < 1.605$ and the maximum value of the exchange integral is obtained for $p/n_i \approx 0.548$. We took into consideration only the first oscillating cycle of the function in Eq. (5), since the subsequent oscillations are expected to be damped by a decorrelation term accounting for inelastic scattering of charge carriers. Alternatively, Eq. (5) may also be integrated by considering all interactions of a spin S_1 with all spins S_2 distributed into the solid with a density n_i. The integral should be performed from a lower distance between impurities $R_0 \approx \{3/(4\pi n_i)\}^{1/3}$. Starting with $J_{12}(r)$ given by Eq. (3), one obtains:

$$J_{tot.} = n_i \int d^3r J_{12}(r) = \left(\frac{\pi}{6}\right)^{1/3}\frac{|\Delta|^2 m^* {n_i}^{4/3}}{h^2} sin\left[\left(\frac{18\pi p}{n_i}\right)^{1/3}\right] \quad (6)$$

In this case, ferromagnetism is obtained for $p/n_i < \pi^2/18 \approx 0.548$, and the maximum value of the exchange integral is given by $p/n_i < \pi^2/144 \approx 0.069$. Note also that a more sophisticated Monte-Carlo simulation, including damping, yielded $p/n_i > 0.1$ or even 0.25 [71].

In the actual case, near surface the Mn density is about $n_i \approx 0.85/(64\,Å^3) \approx 1.3 \times 10^{28}\,m^{-3}$, the carrier density $p_{max.} \approx 4.5 \times 10^{27}\,m^{-3}$ or $p_{avg.} = 2.3 \times 10^{27}\,m^{-3}$, thus $p/n_i \approx 0.34$ or 0.17. It seems that these ratios, irrespective if we take the maximum or the average hole density, satisfy both that derived from Eq. (5) or from Ref. [69]. Thus, there are also semi-quantitative arguments that may be raised in favor of ferromagnetism intermediated by holes stabilized by the inwards polarization state in the sputtered sample. Once again, sputtering not only served to the creation of Pb vacancies able to generate holes in the material, but also induce defects.

Note also that for perfect compensation of depolarization effects $P \approx ep_{avg.}\delta_h$ (see Fig. 1). Taking a robust polarization of PZT of this range of thicknesses (1 Cm^{-2} [29]), one obtains $\delta_h \approx 2.8$ nm, in good agreement with previous estimations [22]. This value exceeds the IMFP of the photoelectrons, thus it confirms a posteriori the validity of this method to assess the surface band bending. One further comment concerns the fact that in a recent estimate of $P^{(-)}$ polarized PZT films, a value of about 2 Å was obtained for this parameter [45], i.e. about one order of magnitude lower. But in this case strong oxygen deficit was found by XPS analysis near the sample surface (the ratio between oxygen and all cations was about 0.9 instead of 1.5) and most probably the established charge sheet for compensation is formed by ionized donors, with a larger charge density confined in a lower thickness than holes treated in the free particle approximation, supposed by eq. (2).

Also, the obtained value for δ_h in the range of 3 nm may give us an estimate of the thickness of the ferromagnetic layer. In fact, by using the MOKE penetration depth of $3\lambda \approx 15$–20 nm (λ being the parameter of the exponential decay of the magnetic signal originating from a deeper layer) and assuming that only the outer 3 nm are ferromagnetic, the observed Mn magnetic moment has to be recalibrated by dividing it to $1 - \exp.(-\delta_h/\lambda)$. Introducing here the 'observed' value of 1.4 Bohr magnetons and $\lambda = 5$–6.7 nm, one obtains Mn atomic moments in the range of 3.1–3.9 Bohr magnetons, which is amongst the highest values ever reported for Mn in a diluted ferromagnetic system. Nevertheless, this estimate is based on the hypothesis that only the surface layer where holes are present is responsible for the whole ferromagnetic signal.

One last evaluation concerns the order of magnitude of the RKKY exchange interaction. The main difficulty is to estimate the Δ matrix elements. A reasonable estimate of its order of magnitude is of a few Hartree $\times$ 4π(Bohr radius)$^3/3$. Using the above values of n_i and the free electron mass, the pre-factor of Eq. (5) yields about 2.4 meV $\times$ $|\Delta|^2$ in the above units. Next, the Curie temperature in the Weiss model is given by $k_B T_C = (2/3)\ S(S+1)\ J_{tot.}$ [72], where $J_{tot.}$ is the total exchange interaction energy (exchange interaction energy multiplied by the number of nearest neighbors for usual ferromagnetism). For $S = 5/2$ (Mn^{2+}), one obtains a Curie temperature near the room temperature ($\sim$ 250 K) for $|\Delta| = 1$ Hartree $\times$ volume of a sphere with the Bohr radius. It is clear that both the pre-factor in Eq. (5) and the oscillating function influences drastically the establishment of ferromagnetism in such systems. Therefore, theoretical estimates predict correctly the occurrence of ferromagnetism intermediated by holes near the $P^{(-)}$ polarized surface.

There are several next steps of this study to be foreseen. Firstly, one has to certify that indeed there are clear correlations between ferroelectricity ↔ charge accumulation near surface ↔ ferromagnetism induced by indirect exchange. One way to investigate further this phenomenon is to compare temperature dependences of magnetization $M(T)$ and ferroelectric polarization $P(T)$. Indeed, Ref. [18] detected completely different Curie temperatures for ferromagnetism and ferroelectricity for Fe-doped BTO ($T_C^{(FM)} > T_C^{(FE)}$), with no feature in $M(T)$ at the ferroelectric transition temperature. Such experiments are to be foreseen in the future, but one has to supplement this investigation with composition and depth profiling, since it is clear that at 400 °C manganese already has a remarkable mobility into the PZT layer.

Another way to continue this study is to try to $P^{(+)}$ polarize the sample obtained by sputtering, which exhibit ferromagnetism, and check if the ferromagnetism is still there after the polarization change. This implies the deposition of a thin nonmagnetic electrode, such as to use it for poling, but to be able to investigate by MOKE the underlying Mn-doped PZT layer.

Finally, measurements of $M(T)$ and $P(T)$ at lower temperatures could also help in establishing a clear connection between ferromagnetism and ferroelectricity, together with correlated PFM and magnetic force microscopy (MFM), investigations of samples with a wider range of Mn content, etc.

5. Conclusions

There are serious arguments to think that the observed ferromagnetism at room temperature in a thin film obtained by Mn deposition at high temperature on a PZT film after a sputtering and annealing procedure is connected with the observed inwards oriented polarization. This polarization orientation stabilizes a hole sheet near the surface, in the region where Mn ions are diffused, and these carriers intermediate ferromagnetism by indirect exchange. Mn deposition on a film without sputtering did not result in room temperature ferromagnetism, which can be due to the different polarization state observed in this film, but also to limited Mn diffusion and to the formation of a stable Mn oxide on the surface. To form this oxide, Mn uptakes oxygen from the substrate, contributing to the creation of oxygen vacancies, which are donors and produce charge carriers to stabilize the outwards polarization orientation.

Some theoretical semi-quantitative estimates based on RKKY theory confirmed that at least concerning the orders of magnitude, the ratio between hole density and the impurity concentration is in the range where one might expect ferromagnetism induced by double exchange. The total exchange interaction itself may reach vigorous values to provide a Curie temperature above the room temperature. Though not definitive, all the indications provided by XPS, MOKE, PFM and theoretical estimate converge to an interplay between ferromagnetism and ferroelectricity, where the hole accumulated near surface to compensate the depolarization field play a central role.

Acknowledgments

This work is funded by the Romanian Ministry for Research and Innovation through the NIMP Core Program PN18-11/2018 and by the UEFISCDI Agency through Projects PN-III-P1-1.1-PD-2016-1322 and PN-III-P1-1.2-PCCDI-2017-0152 (Contract No. 75PCCDI/2018).

Author contributions

CMT had the idea of this experiment, lead it and conceived the manuscript. LP assisted in the elaboration of the manuscript and lead the preparation and basic characterization of these samples. The samples were prepared by CFC using PLD. PFM and AFM analyses were performed by LT. ICB, NGA, LEA, CAT, and RMC performed the MBE depositions and characterization by photoelectron spectroscopy. ICB and CAT performed the MOKE measurements. Photoemission data analysis by 'deconvolution' and final assignments were performed by ICB and CMT.

References

[1] L.W. Martin, Y.H. Chu, R. Ramesh, Advances in the growth and characterization of magnetic, ferroelectric, and multiferroic oxide thin films, Mater. Sci. Eng. Rep. 68 (2010) 89–133.
[2] N.A. Hill, Why are there so few magnetic ferroelectrics? J. Phys. Chem. B 104 (2000) 6694–6709.
[3] J.G. Wu, Z. Fan, D.Q. Xiao, J.G. Zhu, J. Wang, Multiferroic bismuth ferrite-based materials for multifunctional applications: ceramic bulks, thin films and nanostructures, Prog. Mater. Sci. 84 (2016) 335–402.
[4] J.-M. Hu, L.-Q. Chen, C.-W. Nan, Multiferroic heterostructures integrating ferroelectric and magnetic materials, Adv. Mater. 28 (2016) 15–39.
[5] C. Zener, Interaction between d shells in the transition metals, Phys. Rev. 81 (1951) 299–301.
[6] T. Dietl, H. Ohno, F. Matsukura, J. Cibert, D. Ferrand, Zener model description of ferromagnetism in zinc-blende magnetic semiconductors, Science 287 (2000) 1019–1022.
[7] M.A. Ruderman, C. Kittel, Indirect exchange coupling of nuclear magnetic moments by conduction electrons, Phys. Rev. 96 (1954) 99–102.
[8] T. Kasuya, A theory of metallic ferro- and antiferromagnetism on Zener's model, Progr. Theor. Phys. 16 (1956) 45–57.
[9] K. Yosida, Magnetic properties of Cu-Mn alloys, Phys. Rev. 106 (1957) 893–898.
[10] J.M.D. Coey, M. Venkatesan, C.B. Fitzgerald, Donor impurity band exchange in dilute ferromagnetic oxides, Nat. Mater. 4 (2005) 173–179.
[11] Y.-H. Lin, J.C. Yuan, S.Y. Zhang, Y. Zhang, J. Liu, Y. Wang, C.-W. Nan, Multiferroic behavior observed in highly orientated Mn-doped $BaTiO_3$ thin films, Appl. Phys. Lett. 95 (2009) 033105.
[12] R.V.K. Mangalam, M. Chakrabrati, D. Sanyal, A. Chakrabati, A. Sundaresan, Identifying defects in multiferroic nanocrystalline $BaTiO_3$ by positron annihilation techniques, J. Phys. Cd. Mat. 21 (2009) 445902.
[13] T. Dietl, H. Ohno, Dilute ferromagnetic semiconductors: physics and spintronic structures, Rev. Mod. Phys. 86 (2014) 187–251.
[14] T. Dietl, A. Haury, Y. Merle D'Aubigné, Free carrier-induced ferromagnetism in structures of diluted magnetic semiconductors, Phys. Rev. B 55 (1997) R3347–R3350.
[15] H. Nakayama, H. Katayama-Yoshida, Theoretical prediction of magnetic properties of $Ba(Ti_{1-x}M_x)O_3$ (M = Sc, V, Cr, Mn, Fe, Co, Ni, Cu), Jpn. J. Appl. Phys. 40 (2001) L1355–L1358.
[16] J.S. Lee, Z.G. Khim, Y.D. Park, D.P. Norton, N.A. Theodoropoulou, A.F. Hebard, J.D. Budai, L.A. Boatner, S.J. Pearton, R.G. Wilson, Magnetic properties of Co- and Mn-implanted $BaTiO_3$, $SrTiO_3$ and $KTaO_3$, Solid State Electron. 47 (2003) 2225–2230.

[17] X.R. Tong, Y.-H. Lin, S.Y. Zhang, Y. Wang, C.-W. Nan, J. Appl. Phys. 104 (2008) 066108.
[18] B. Xu, K.B. Yin, J. Lin, Y.D. Xia, X.G. Wan, J. Yin, X.J. Bai, J. Du, Z.G. Liu, Room-temperature ferromagnetism and ferroelectricity in Fe-doped $BaTiO_3$, Phys. Rev. B 79 (2009) 134109.
[19] Y. Shuai, S.Q. Zhou, D. Bürger, H. Reuther, I. Skorupa, V. John, M. Helm, H. Schmidt, Decisive role of oxygen vacancy in ferroelectric versus ferromagnetic Mn-doped $BaTiO_3$ thin films, J. Appl. Phys. 109 (2011) 084105.
[20] A. Boonchun, M.F. Smith, B. Cherdhirunkorn, S. Limpijumnong, First principles study of Mn impurities in $PbTiO_3$ and $PbZrO_3$, J. Appl. Phys. 101 (2007) 043521.
[21] L. Pintilie, M. Alexe, Metal-ferroelectric-metal heterostructures with Schottky contacts. I. Influence of the ferroelectric properties, J. Appl. Phys. 98 (2005) 124103.
[22] L. Pintilie, I. Boerasu, M.J.M. Gomes, T. Zhao, R. Ramesh, M. Alexe, Metal-ferroelectric-metal structures with Schottky contacts. II. Analysis of the experimental current-voltage and capacitance-voltage characteristics of $Pb(Zr,Ti)O_3$ thin films, J. Appl. Phys. 98 (2005) 124104.
[23] L.E. Ştoflea, N.G. Apostol, L. Trupină, C.M. Teodorescu, et al., J. Mater. Chem. A 2 (2014) 14386–14392.
[24] L.C. Tănase, N.G. Apostol, L.E. Abramiuc, C.A. Tache, L. Hrib, L. Trupină, L. Pintilie, C.M. Teodorescu, Ferroelectric triggering of carbon monoxide adsorption on lead zirco-titanate (001) surfaces, Sci. Rep. 6 (2016) 35301.
[25] N.G. Apostol, G.A. Lungu, I.C. Bucur, C.A. Tache, L. Hrib, L. Pintilie, D. Macovei, C.M. Teodorescu, Non-interacting, sp^2 hybridized carbon layers on ferroelectric lead zirco-titanate, RSC Adv. 6 (2016) 67883–67887.
[26] N.G. Apostol, L.E. Ştoflea, L.C. Tănase, I.C. Bucur, C. Chirilă, R.F. Negrea, C.M. Teodorescu, Band bending at copper and gold interfaces with ferroelectric Pb(Zr,Ti)O_3 investigated by photoelectron spectroscopy, Appl. Surf. Sci. 354 (2015) 459–468.
[27] L.C. Tănase, L.E. Abramiuc, C.M. Teodorescu, Photoelectron spectroscopic and microspectroscopic probes of ferroelectrics, AIP Conf. Proc. 1916 (2017) 030001.
[28] I.C. Bucur, L.C. Tănase, L.E. Abramiuc, G.A. Lungu, C. Chirilă, L. Trupină, N.G. Apostol, R.M. Costescu, L. Pintilie, C.M. Teodorescu, Triggering surface ferroelectric order in $Pb(Zr,Ti)O_3(001)$ by deposition of platinum, Appl. Surf. Sci. 432 (2018) 27–33.
[29] L. Pintilie, C. Ghica, C.M. Teodorescu, I. Pintilie, C. Chirila, I. Pasuk, L. Trupina, L. Hrib, A.G. Boni, N.G. Apostol, L.E. Abramiuc, R. Negrea, M. Stefan, D. Ghica, Polarization induced self-doping in epitaxial $Pb(Zr_{0.20}Ti_{0.80})O_3$ thin films, Sci. Rep. 5 (2015) 14974.
[30] S. Limpijumnong, S. Rujirawat, A. Boonchun, M.F. Smith, B. Cherdhirunkorn, Identification of Mn site in $Pb(Zr,Ti)O_3$ by synchrotron x-ray absorption near-edge structure: theory and experiment, Appl. Phys. Lett. 90 (2007) 103113.
[31] L.X. He, C.E. Li, Effects of addition of MnO on piezoelectric properties of lead zirconate titanate, J. Mater. Sci. 35 (2000) 2477–2480.
[32] I. Pintilie, C.M. Teodorescu, C. Ghica, C. Chirila, A.G. Boni, L. Hrib, I. Pasuk, R. Negrea, N.G. Apostol, L. Pintilie, Polarization-control of the potential barrier at the electrode interfaces in epitaxial ferroelectric thin films, ACS Appl. Mater. Interface 6 (2014) 2929–2939.
[33] L. C. Tănase, L. E. Abramiuc, D. G. Popescu, A.-M. Trandafir, N. G. Apostol, I. C. Bucur, L. Hrib, L. Pintilie, C. M. Teodorescu, Polarization orientation in lead zirco-titanate (001) thin films driven by the interface with the substrate, L.C. Tănase, L.E. Abramiuc, Phys. Rev. Applied Vol. 10 (2018) 034020.
[34] G.A. Lungu, N.G. Apostol, L.E. Stoflea, R.M. Costescu, D.G. Popescu, C.M. Teodorescu, Room temperature ferromagnetic, anisotropic, germanium rich FeGe(001) alloys, Materials 6 (2013) 612–625.
[35] G.A. Lungu, L.E. Stoflea, L.C. Tănase, I.C. Bucur, N. Răduţoiu, F. Vasiliu, I. Mercioniu, V. Kuncser, C.M. Teodorescu, Room temperature ferromagnetic Mn:Ge (001), Materials 7 (2014) 106–129.
[36] L.C. Tănase, G.A. Lungu, L.E. Abramiuc, I.C. Bucur, N.G. Apostol, R.M. Costescu, C.A. Tache, D. Macovei, A. Barinov, C.M. Teodorescu, Long range magnetic interaction in Mn_xGe_{1-x}: structural, spectro-microscopic and magnetic investigations, J. Mater. Sci. 52 (2017) 3309–3320.
[37] N.G. Apostol, L.E. Stoflea, G.A. Lungu, C.A. Tache, D.G. Popescu, L. Pintilie, C.M. Teodorescu, Band bending at free $Pb(Zr,Ti)O_3$ surfaces analyzed by X-ray photoelectron spectroscopy, Mater. Sci. Eng. B 178 (2013) 1317–1322.
[38] F. Chen, R. Schafranek, W.B. Wu, A. Klein, Reduction-induced Fermi level pinning at the interfaces between $Pb(Zr,Ti)O_3$ and Pt, Cu and Ag metal electrodes, J. Phys. D. Appl. Phys. 44 (2011) 255301.
[39] F. Chen, A. Klein, Polarization dependence of Schottky barrier heights at interfaces of ferroelectrics determined by photoelectron spectroscopy, Phys. Rev. B 86 (2012) 094105.
[40] N.G. Apostol, L.E. Stoflea, G.A. Lungu, C. Chirila, L. Trupina, R.F. Negrea, C. Ghica, L. Pintilie, C.M. Teodorescu, Charge transfer and band bending at $Au/Pb(Zr,Ti)O_3$ interfaces investigated by photoelectron spectroscopy, Appl. Surf. Sci. 273 (2013) 415–425.
[41] N.G. Apostol, L.E. Stoflea, G.A. Lungu, L.C. Tanase, C. Chirila, L. Frunza, L. Pintilie, C.M. Teodorescu, Band bending in $Au/Pb(Zr,Ti)O_3$ investigated by X-ray photoelectron spectroscopy: dependence on the initial state of the film, Thin Solid Films 545 (2013) 13–21.
[42] L.E. Stoflea, N.G. Apostol, C. Chirila, L. Trupina, R. Negrea, L. Pintilie, C.M. Teodorescu, Schottky barrier versus surface ferroelectric depolarization at $Cu/Pb(Zr,Ti)O_3$ interfaces, J. Mater. Sci. 49 (2014) 3337–3351.
[43] D.G. Popescu, M.A. Huşanu, L. Trupină, L. Hrib, L. Pintilie, A. Barinov, S. Lizzit, P. Lacovig, C.M. Teodorescu, Spectro-microscopic photoemission evidence of charge uncompensated areas in $Pb(Zr,Ti)O_3(001)$ layers, Phys. Chem. Chem. Phys. 17 (2015) 509–520.
[44] L.E. Abramiuc, L.C. Tănase, A. Barinov, N.G. Apostol, C. Chirilă, L. Trupină, L. Pintilie, C.M. Teodorescu, Polarization landscape effects in soft X-ray-induced surface chemical decomposition of lead zirco-titanate, evidenced by photoelectron spectromicroscopy, Nanoscale 9 (2017) 11055–11067.
[45] C.M. Teodorescu, L. Pintilie, N.G. Apostol, R.M. Costescu, G.A. Lungu, L. Hrib, L. Trupină, L.C. Tănase, I.C. Bucur, A.E. Bocîrnea, Low energy electron diffraction from ferroelectric surfaces. Dead layers and surface dipoles in ultraclean $Pb(Zr,Ti)O_3(001)$, Phys. Rev. B 96 (2017) 115438.
[46] M. Prabu, I.B. Shameem Banu, S. Tiripura Sundari, R. Krishnan, K. Niranjan Prakash, Y.C. Chen, M. Chavali, Optical studies of pulsed laser deposited nanostructured $Pb(Zr_{0.52}Ti_{0.48})O_3$ thin film by spectroscopic ellipsometry, J. Nanosci. Nanotechnol. 14 (2014) 5335–5341.
[47] C.M. Teodorescu, F. Chevrier, R. Brochier, C. Richter, O. Heckmann, V. Ilakovac, P. De Padova, K. Hricovini, X-ray magnetic circular dichroism, photoemission and RHEED studies of Fe/InAs(100) interfaces, Surf. Sci. 482–485 (2001) 1004–1009.
[48] C.M. Teodorescu, F. Chevrier, R. Brochier, V. Ilakovac, O. Heckmann, L. Lechevalier, K. Hricovini, Reactivity and magnetism of Fe/InAs(100) interfaces, Eur. Phys. J. B 28 (2002) 305–313.
[49] C.M. Teodorescu, J.M. Esteva, R.C. Karnatak, A. El Afif, An approximation of the Voigt I profile for the fitting of experimental X-ray absorption data, Nucl. Instrum. Methods Phys. Res. A 345 (1994) 141–147.
[50] D. Mardare, D. Luca, C.M. Teodorescu, D. Macovei, On the hydrophilicity of nitrogen-doped TiO_2 thin films, Surf. Sci. 601 (2007) 4515–4520.
[51] D. Luca, C.M. Teodorescu, R. Apetrei, D. Macovei, D. Mardare, Preparation and characterization of increased-efficiency photocatalytic $TiO_{2-2x}N_x$ thin films, Thin Solid Films 515 (2007) 8605–8610.
[52] M. Oku, K. Hirokawa, S. Ikeda, X-ray photoelectron spectroscopy of manganese-oxygen systems, J. Electron Spectrosc. Relat. Phenom. 7 (1975) 465–473.
[53] V. Di Castro, G. Polzonetti, XPS study of MnO oxidation, J. Electron Spectrosc. Relat. Phenom. 48 (1989) 117–123.
[54] A.V. Naumkin, A. Kraut-Vass, S.W. Gaarenstroom, C.J. Powell, NIST X-ray Photoelectron Spectroscopy Database / NIST Standard Reference Database 20, Version 4.1, https://srdata.nist.gov/xps , Accessed date: 21 November 2017.
[55] A. Pancotti, J. Wang, P. Chen, L. Tortech, C.M. Teodorescu, E. Frantzeskakis, N. Barrett, X-ray photoelectron diffraction study of relaxation and rumpling of ferroelectric domains in $BaTiO_3(001)$, Phys. Rev. B 87 (2013) 184116.
[56] M. Iliut, C. Leordean, V. Canpean, C.M. Teodorescu, S. Astilean, A new green, ascorbic acid-assisted method for versatile synthesis of Au-graphene hybrids as efficient surface-enhanced Raman scattering platforms, J. Mater. Chem. C 1 (2013) 4094–4104.
[57] C.D. Wagner, L.E. Davis, M.V. Zeller, J.A. Taylor, R.H. Raymond, L.H. Gale, Empirical atomic sensitivity factor for quantitative analysis by electron spectroscopy for chemical analysis, Surf. Interf. Anal. 3 (1981) 211–225.
[58] M.P. Seah, W.A. Dench, Quantitative electron spectroscopy of surfaces: a standard data base for electron inelastic mean free paths in solids, Surf. Interface Anal. 1 (1979) 2.
[59] F. Zavaliche, W. Wulfhekel, H. Xu, J. Kirschner, Suppression of silicide formation in Fe films grown on Si(001), J. Appl. Phys. 88 (2000) 5289–5292.
[60] V. Kuncser, W. Keune, U. von Hörsten, G. Schinteie, Interlayer magnetic coupling in exchange bias and spin valve structures with Fe-Mn and Ir-Mn antiferromagnetic layers, J. Optoelectron. Adv. Mater. 12 (2010) 1385–1393.
[61] R.M. Costescu, N.G. Gheorghe, M.A. Husanu, G.A. Lungu, D. Macovei, I. Pintilie, D.G. Popescu, C.M. Teodorescu, Epitaxial ferromagnetic samarium and samarium silicide synthesized on Si(001), J. Mater. Sci. 47 (2012) 7225–7234.
[62] K. Hricovini, P. De Padova, C. Quaresima, P. Perfetti, R. Brochier, C. Richter, V. Ilakovac, O. Heckmann, L. Lechevallier, P. Bencok, P. Le Fevre, C. Teodorescu, Atomic structure and magnetic properties of Mn on InAs(100), Appl. Surf. Sci. 212–213 (2003) 17–25.
[63] A. Quesada, M.A. Garcia, M. Andres, A. Hernando, J.F. Fernandez, A.C. Caballero, M.S. Martin-Gonzalez, F. Briones, Ferromagnetism in bulk Co-Zn-O, J. Appl. Phys. 100 (2006) 113909.
[64] M.S. Martín-González, J.F. Fernández, F. Rubio-Marcos, I. Lorite, J.L. Costa-Krämer, A. Quesada, M.A. Bañares, J.L.G. Fierro, Insights into the room temperature magnetism of ZnO/Co_3O_4 mixtures, J. Appl. Phys. 103 (2008) 083905.
[65] M.V. Kuznetsov, J.F. Zhuravlev, V.A. Gubanov, XPS analysis of adsorption of oxygen molecules on the surface of Ti and TiN_x films in vacuum, J. Electr. Spectrosc. Relat. Phenom. 58 (1992) 169–176.
[66] S.A. Chambers, F. Xu, H.W. Chen, I.M. Vitomirov, S.B. Anderson, J.H. Weaver, Simultaneous epitaxy and substrate out-diffusion at a metal-semiconductor interface: Fe/GaAs(001)-c(8×2), Phys. Rev. B 34 (1986) 6605–6611.
[67] M.W. Ruckman, J.J. Joyce, J.H. Weaver, Interdiffusion and reaction at the Fe/GaAs (110) interface, Phys. Rev. B 33 (1986) 7029–7035.
[68] C.M. Teodorescu, D. Luca, Comparative study of magnetism and interface composition in Fe/GaAs(100) and Fe/InAs(100), Surf. Sci. 600 (2006) 4200–4204.
[69] D.R. Lide, et al. (Ed.), CRC Handbook of Chemistry and Physics, 75th Edition, CRC Press, Boca Raton, 1994, pp. 51–56.
[70] T. Shimada, T. Ueda, J. Wang, T. Kitamura, Hybrid Hartree-Fock density functional study of charged point defects in ferroelectric $PbTiO_3$, Phys. Rev. B 87 (2013) 174111.
[71] D.J. Priour Jr., S. Das Sarma, Phase diagram of the disordered RKKY model in dilute magnetic semiconductors, Phys. Rev. Lett. 97 (2006) 127201.
[72] C. Kittel, Introduction to Solid State Physics, Eigth Edition, Wiley, Hoboken, 2005, p. 325.